Geochemistry Geophysics Geosystems G3
AN ELECTRONIC JOURNAL OF THE EARTH SCIENCES
Published by AGU and the Geochemical Society

*Article*
Volume 10, Number 5
16 May 2009
Q05005, doi:10.1029/2009GC002403
ISSN: 1525-2027



# Isotope fractionation and mixing in methane plumes from the Logatchev hydrothermal field

**Robin S. Keir**
*Leibniz-Institut für Meereswissenschaften an der Universität Kiel (IFM-GEOMAR), Dienstgebäude Ostufer, Wischhofstraße 1-3, D-24148 Kiel, Germany (rkeir@ifm-geomar.de)*

**Oliver Schmale**
*Sektion Meereschemie, Institut für Ostseeforschung Warnemünde, Seestraße 15, D-18119 Rostok-Warnemünde, Germany*

**Richard Seifert**
*Institut für Biogeochemie und Meereschemie, Universität Hamburg, Bundesstraße 55, D-20146 Hamburg, Germany*

**Jürgen Sültenfuß**
*Institut für Umweltphysik, Universität Bremen, Otto-Hahn-Allee 1, Gebäude NW1, D-28359 Bremen, Germany*

[1] As methane is consumed in the deep sea, its $^{13}C/^{12}C$ ratio progressively increases because of kinetic isotope fractionation. Many submarine hydrothermal vents emit methane with carbon isotope ratios that are higher than those of background methane in the surrounding ocean. Since the latter exists at low concentrations, mixing of background methane with vent fluid tends to decrease the $^{13}C/^{12}C$ ratio as concentration decreases, opposite to the trend produced by consumption. We investigated $CH_4$ concentration and $\delta^{13}C$ together with $\delta^3He$ in plumes from the Logatchev hydrothermal field (LHF) located at 14°45′N, 45°W, which generates relatively heavy methane ($\delta^{13}C \approx -13‰$) by serpentinization of ultramafic rock. The measured methane and $\delta^3He$ were well correlated at high concentrations, indicating a $CH_4/^3He$ ratio of $1 \times 10^8$ in the vent fluids. These tracer distributions were also simulated with an advection-diffusion model in which methane consumption only occurs above a certain threshold concentration. We utilized $\delta^3He$ to calculate the methane remaining in solution after oxidation, $f$, and the deviation of $\delta^{13}C$ from the value expected from mixing alone, $\Delta\delta^{13}C$. Both in the model and in the data, the entire set of $\Delta\delta^{13}C$ values are not correlated with $\log f$, which is due to continuous oxidation within the plume while mixing with background seawater. A linear relationship, however, is found in the model for methane at concentrations sufficiently above background, and many of the samples with elevated $CH_4$ north of LHF exhibit a linear trend of $\Delta\delta^{13}C$ versus $\log f$ as well. From this trend, the kinetic isotope fractionation factor in the LHF plumes appears to be about 1.015. This value is somewhat higher than found in some other deep-sea studies, but it is lower than found in laboratory incubation experiments.

**Components:** 11,077 words, 15 figures, 2 tables.

**Keywords:** hydrothermal; isotope fractionation; plumes.

**Index Terms:** 4832 Oceanography: Biological and Chemical: Hydrothermal systems (0450, 1034, 3017, 3616, 8135, 8424); 1041 Geochemistry: Stable isotope geochemistry (0454, 4870); 1009 Geochemistry: Geochemical modeling (3610, 8410).

**Received** 27 January 2009; **Revised** 30 March 2009; **Accepted** 3 April 2009; **Published** 16 May 2009.

Keir, R. S., O. Schmale, R. Seifert, and J. Sültenfuß (2009), Isotope fractionation and mixing in methane plumes from the Logatchev hydrothermal field, *Geochem. Geophys. Geosyst.*, *10*, Q05005, doi:10.1029/2009GC002403.

## 1. Introduction

[2] Fluids emitted from submarine hydrothermal vents are enriched in a variety of compounds that include the dissolved gases, methane, hydrogen and $^3$He. Even after vigorous dilution by ambient seawater during the rise of the hydrothermal effluent, the concentrations of these gases in the resulting neutrally buoyant plume often remain well above those in normal seawater. The absolute amounts and the ratio of these gases to each other in vent fluids vary widely between hydrothermal systems because different processes influence their production. $^3$He flux appears to be coupled to magma production rate at spreading centers [*Farley et al.*, 1995], while methane may be derived from magmatic outgassing, rock-water reactions such as serpentinization of ultramafic rock, and thermogenic production [*Welhan*, 1988; *Charlou et al.*, 1998; *Lilley et al.*, 1993].

[3] The major sinks for these gases are different as well. Helium-3 is conservative within the ocean and is eventually lost to the atmosphere. Methane and hydrogen in the deep ocean, on the other hand, disappear much more quickly because of microbial oxidation. Methane in particular appears to be consumed at various specific rates, even within the lateral plume. From $^{14}CH_4$ incubation experiments, *de Angelis et al.* [1993] determined specific rates between 0.02 and 0.15 day$^{-1}$ in the Endeavor plume, with the maximum rate occurring in samples collected about 2 km away from the vent field. They suggested that a population of methane-oxidizing bacteria develops in the plume and influences the oxidation rate. Estimates of the average specific rate in other methane plumes range from 0.002 to 0.01 day$^{-1}$ [*Tsunogai et al.*, 2000; *Valentine et al.*, 2001; *Keir et al.*, 2008]. In newly formed deep waters, the turnover time appears to be much longer, on the order of decades [*Rehder et al.*, 1999; *Heeschen et al.*, 2004; *Keir et al.*, 2005]. In the bulk of the deep ocean, methane never disappears completely and retains a low, relatively constant "background" concentration of 0.4 to 0.5 nM in the Atlantic and 0.2 to 0.3 nM in the Pacific [*Charlou and Donval*, 1993]. Thus, it appears that once the concentration reaches this level, microbial oxidation virtually ceases [*Scranton and Brewer*, 1978].

[4] Isotope measurements have shown that the $^{13}C/^{12}C$ ratio of methane increases in aging hydrothermal plumes [*Tsunogai et al.*, 2000; *Cowen et al.*, 2002], which is due to the slightly faster consumption of $^{12}CH_4$ relative to that of $^{13}CH_4$. If the kinetic isotope effect is known, one can in principal assess the extent of microbial methane oxidation from the distribution of the carbon isotope ratios [e.g., *Valentine et al.*, 2001; *Tsunogai et al.*, 2005] using the closed system Rayleigh model of isotope fractionation [e.g., *Coleman et al.*, 1981]. Two difficulties in applying this model are that (1) kinetic isotope fractionation in natural seawater environments is not completely understood and (2) the plume is not a closed system in that the isotope ratios are also affected by continuous mixing with surrounding water as the plume advects and disperses.

[5] In regard to the first point above, relatively low isotope fractionation factors ($\alpha$ = 1.004 to 1.01) have been derived from several field studies of methane carbon isotopes in the cold environment of the intermediate and deep ocean [*Tsunogai et al.*, 2000; *Cowen et al.*, 2002; *Grant and Whiticar*, 2002; *Heeschen et al.*, 2004]. This might occur if microbial isotope fractionation decreases with decreasing temperature, as suggested by *Coleman et al.* [1981] on the basis of their incubation experiments. Other workers emphasize the role of methantrophic bacterial cell density [*Templeton et al.*, 2006; *Kinnaman et al.*, 2007]. The continuous flow experiments of *Templeton et al.* [2006] indicate that greater fractionation occurs at low cell densities and high methane concentrations, whereas at high densities and low concentrations, almost no fractionation occurs. The latter is ascribed to "diffusion limitation" into the bacterial cells. Whether such substrate limitation affects isotope fractionation in open ocean environments is not known.

[6] Aside from the question of variable fractionation, mixing of plume and ambient water adds another complication to the interpretation of oceanographic methane carbon isotope ratios. When the source $\delta^{13}C$ is heavier than in the background methane, which is the case in many submarine hydrothermal systems, mixing and oxidation produce opposite effects on the trend of the isotopic ratio as the concentration decreases. In order to examine these effects, we surveyed methane, its

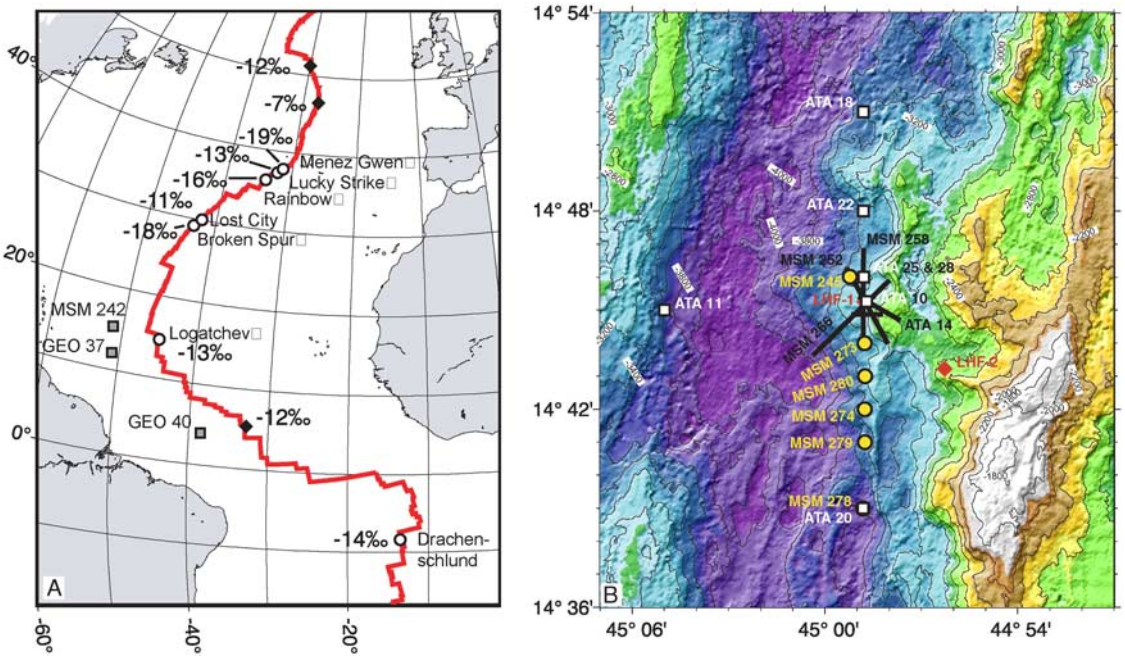


**Figure 1.** (a) Location of Logatchev and other hydrothermal vents (circles) on the Mid-Atlantic Ridge axis (red line). Diamonds indicate locations of methane plumes for which the source has not been identified. Adjacent numbers indicate $\delta^{13}$C of methane in the vent fluids/plumes (compiled by *Charlou et al.* [2002]; also *Keir et al.* [2005, 2008]). Squares show locations of off-axis GEOSECS and *Merian* 4/3 stations. (b) Location of hydrocast stations on *Merian* 4/3 and *L'Atalante*. Vertical cast positions indicated by circles (R/V *Merian*) and squares (R/V *L'Atalante*). Lines indicate tow-yo tracks.

carbon isotope ratio and $^3$He in the vicinity of the main Logatchev hydrothermal field (LHF-1) at 14°45′N on the Mid-Atlantic Ridge (MAR). As an aid to interpreting this data, we also simulated these tracers according to constant advection, diffusion and isotope fractionation in a model with discontinuous first-order kinetics of methane oxidation. We then use the distribution of $^3$He, a conservative tracer, to estimate the extent of methane consumption and degree of isotope fractionation, both in the observed data and in the model. The latter provides some foundation as to the reliability of this procedure.

[7] Discovery of the Logatchev hydrothermal field was the result of several Russian expeditions during the mid-1990s [*Cherkaschev et al.*, 2000; *Sudarikov and Roumiantsev*, 2000]. LHF is one of six known high-temperature vent fields on the MAR that are hosted in gabbroic and ultramafic rock. Vent fluids from the main field were first sampled during the French MICROSMOKE expedition in 1996 [*Douville et al.*, 2002]. The fluids contain high concentrations of hydrogen (~16 mM) and methane (~3 mM) [*Charlou et al.*, 2002; *Schmidt et al.*, 2007], apparently due to serpentinization of the mantle rock [*Charlou et al.*, 1998]. The $\delta^{13}$C of the methane emitted from the various vents at LHF-1 appears to have remained almost constant since it was first measured by *Lein et al.* [2000]. They reported $\delta^{13}$C values between −13.8 and −14.6‰. During the German Priority Program 1144, methane $^{13}$C/$^{12}$C ratio was measured in vent fluid samples collected at various sites during the period between February 2004 and December 2007. The average and standard deviation of $\delta^{13}$C measurements on each site is given in Table 1. These values (site average $\delta^{13}$C = −12.8 ± 0.8‰) are typical of hydrothermal vent fluids and plumes investigated elsewhere on the MAR (Figure 1a) and are heavier than in methane from biogenic or thermogenic sources [*Welhan*, 1988; *Lilley et al.*, 1993]. LHF-1 is located on the eastern side of the rift valley and consists of at least six active vent sites lined up over a distance of about 600 m. Although these sites exhibit a diversity of venting styles, from diffuse to black smokers, the end-member concentrations of major and most trace elements are similar at all of the vents, indicating a common source in the reaction zone [*Schmidt et al.*, 2007].

[8] Previous work indicated that fluids emanating from the LHF-1 reach different heights above the bottom because of the different types of venting [*Sudarikov and Roumiantsev*, 2000; *Zhou et al.*, 2007; H. Marbler et al., Distribution and structure of the black smoker plume at Logatchev hydro-

**Table 1.** Average $\delta^{13}C$ of Methane of Vent Fluid at Various Logatchev Sites[a]

| Site Designation | Average $\delta^{13}C$ (‰) | Number of Samples |
|---|---|---|
| Irina 2[b] | −12.8 ± 1.2 | n = 16 |
| Site B | −13.0 ± 0.8 | n = 5 |
| Irina 1 | −12.0 ± 0.7 | n = 8 |
| Quest[b] | −13.8 ± 0.8 | n = 9 |
| Anna Louise | −12.5 | n = 1 |
| Site F | −14.1 | n = 1 |
| Site A | −13.9 ± 0.2 | n = 3 |
| Smokey Strobe | −12.0 | n = 1 |
| Candelabra | −11.8 | n = 1 |
| Site average | −12.8 ± 0.8 | |

[a] Samples were collected during the expeditions *Meteor* 60/3 and 64/2, *M. S. Merian* 4/3, and *L'Atalante*.
[b] Measurements of fluids diffusing through mussel beds not included.

thermal field at 14°45′N at the Mid-Atlantic Ridge, paper presented at 3rd Annual SPP 1144 Workshop, Deutsche Forschungsgemeinschaft, Etelsen, Germany, 4–6 July 2006, available at http://www.ifm-geomar.de/fileadmin/ifm-geomar/fb4/fb4_fe2/spetersen/Etelsen2006_Abstracts.pdf]. The uppermost plume rises to a depth of about 2750 m (ca. 250 m above the vents) before spreading horizontally, while a second plume stays low over the bottom, rising no more than 30 or 40 m above the vents. *Sudarikov and Roumiantsev* [2000] suggested that this plume might contain brine due to vapor separation in the hydrothermal circulation and thus flow downslope as a "reverse plume." However, analyses of vent fluids at LHF-1 so far have not shown enhanced chloride concentrations [*Schmidt et al.*, 2007]. In contrast, active venting has recently been found 5 km to the southeast of the main field at a site designated LHF-2 (position in Figure 1b), and these fluids have low chloride content [*Fouquet et al.*, 2008]. West and northwest of the main field, methane anomalies have been reported near the bottom at depths (∼3200 m) greater than those of the known vents [*Zhou et al.*, 2007; Marbler et al., presented paper, 2006]. Whether this might be due to a downslope-flowing plume from the main vent field or to an additional vent(s) located at deeper depths is not known.

## 2. Methods

### 2.1. Sampling

[9] Water column samples were obtained during vertical and tow-yo hydrocasts using CTD/22-bottle Rosette samplers on cruises of R/V *M. S. Merian* 4/3 (23 January to 14 February 2007) and R/V *L'Atalante* (4 December 2007 to 2 January 2008). The majority of the stations were placed on a north-south line crossing the main vent field along the eastern side of the rift valley, on the assumption that this boundary guides the current direction (Figure 1b).

[10] Vent fluids were sampled using remote operated vehicles (ROVs) on 4 research expeditions, *Meteor* 60/3 and 64/2, *M. S. Merian* 4/3 and *L'Atalante*. Different sampling devices were employed on these cruises. On *MSM* 4/3, the vents were sampled with piston-activated titanium (MAJOR) samplers, while on *M60/3, M64/2* and *L'Atalante*, the fluids were obtained by pumping into Teflon cylinders (KIPS) mounted on the ROV [*Schmidt et al.*, 2007]. Neither of these samplers is tight against overpressures that develop from the high gas concentrations in the vent fluids. Loss of gas, however, is not expected to significantly affect the methane carbon isotope measurements as long as this is not accompanied by air contamination. Fluid from the MAJORs was extracted directly into preevacuated 250- and 500-ml bottles. Since the vacuum retracted the piston against the spring tension, it appeared that no air contamination occurred. For the KIPS, air contamination was minimized by opening an air vent at the top of the sampler and immediately drawing a relatively small volume of the fluid into an evacuated bottle through a second vent near the base of the sampler.

### 2.2. Analysis

[11] Seawater samples for helium isotope analysis were collected by crimping copper tubes while flushing with a continuous flow from the Niskin bottle. The $^3He/^4He$ ratio was subsequently determined by mass spectrometry at the University of Bremen according to the method described by *Sültenfuß et al.* [2009].

[12] Methane was analyzed using a partial vacuum extraction method described previously [*Rehder et al.*, 1999; *Keir et al.*, 2005; *Buller*, 2008]. Dissolved gas was extracted into a head space by drawing seawater into evacuated bottles that were filled about two-thirds full. The gas phase was subsequently recompressed to atmospheric pressure and transferred to a gas burette. For water column samples, the volume of seawater taken was monitored with a flowmeter, and the efficiency of gas extraction was estimated from the ratio of observed gas volume to that expected from dissolved $N_2$, Ar and $O_2$. For the *Merian* and *L'Atlante* cruises, the efficiency was 90 ± 6%. The mixing ratio of methane was then analyzed on an aliquot of the extracted gas using a gas

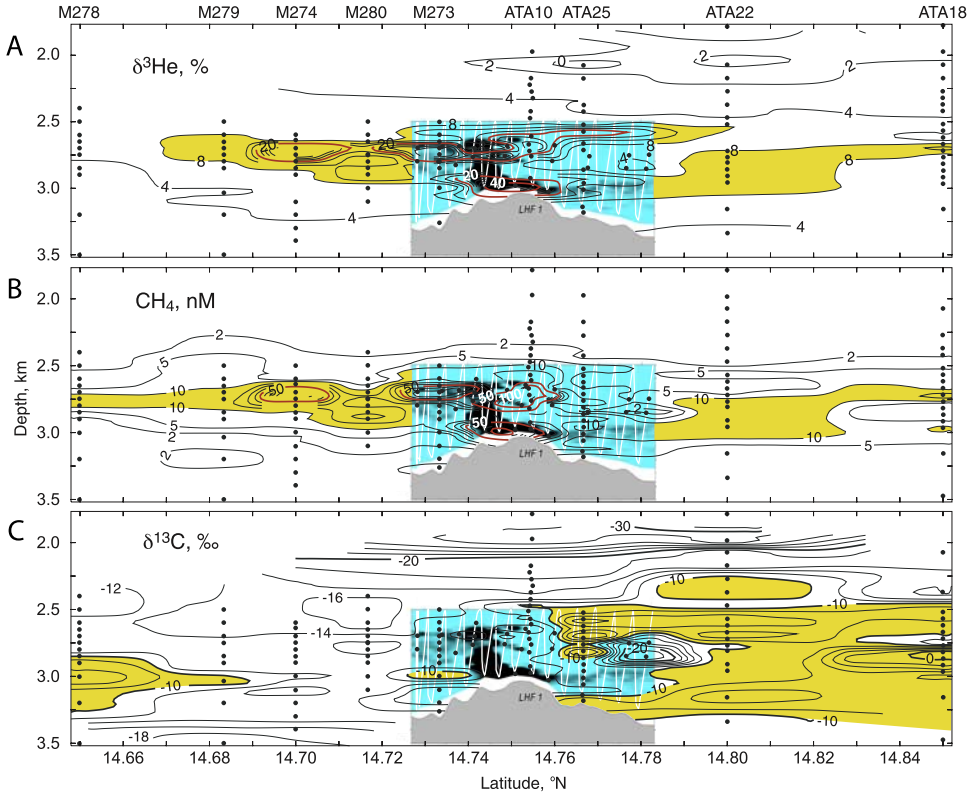


**Figure 2.** North-south sections of (a) $\delta^3$He, (b) $CH_4$ concentration, and (c) $\delta^{13}$C-$CH_4$ over Logatchev-1. These are superimposed on the near-field particle concentration, indicated by the intensity of black on blue, obtained by MAPR measurements during *Merian* tow-yo station 258. The yellow color emphasizes $\delta^3$He > 8% in Figure 2a, [$CH_4$] > 10 nM in Figure 2b, and $\delta^{13}$C-$CH_4$ > −10‰ in Figure 2c. Red contours emphasize high values of $\delta^3$He (20% and 40%) and [$CH_4$] (50 nM and 100 nM).

chromatograph equipped with a flame ionization detector. Propagation of errors indicates that the overall error of the method is ±0.2 nM for [$CH_4$] ≤ 7 nM and ±3% for [$CH_4$] > 7 nM [*Buller*, 2008]. The remainder the gas sample was conserved in 20-ml vials, and the carbon isotope ratio determined with inline ratio monitoring mass spectrometry ashore, as described by *Rice et al.* [2001].

## 3. North-South Distribution of $^3$He, Methane, and Methane $\delta^{13}$C

[13] North-south distributions of $\delta^3$He, methane concentration and methane $\delta^{13}$C over the LHF are shown in Figure 2. The central part of the section includes a tow-yo (MSM Station 258), during which optical backscatter intensity was monitored with miniature autonomous plume recorders (MAPRs; see *Walker et al.* [2004] for description). In each of the sections, particle concentrations (backscatter) from the tow-yo are indicated by the black color intensity. The backscatter data clearly indicate a "split level" structure at the time of the tow-yo, with particle clouds drifting southward between 2700 and 2900 m and a lower plume moving northward near the bottom. As the bottom descends below 3000 m to the north, this plume detaches from the bottom and remains at about constant depth.

[14] The chemical tracer sections in Figure 2 are based on vertical hydrocasts as well as samples captured during the tow-yo. To the south of the vent field, these casts were taken on *M. S. Merian* during the week following the tow-yo, while stations to the north were taken 11 months later on *L'Atalante*. Thus, the spatial distributions are not synoptic and are subject to temporal variations in the current field. Nevertheless, the overall distributions of $\delta^3$He and methane concentration correspond well to the particle plume structure (Figures 2a and 2b). High concentrations of these tracers were found in the upper and lower particle plumes. The upper plume (2750 m) extended southward at least 11 km from the vent field. North of the main vent field, backscatter during the tow-yo indicated relatively clear water at depths above 2800 m. Between about

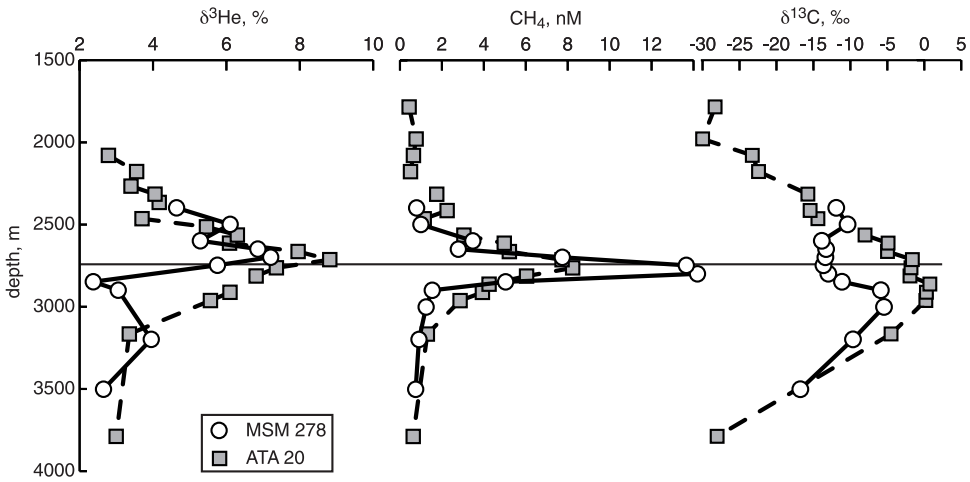


**Figure 3.** The $\delta^3$He, $CH_4$ concentration, and $\delta^{13}$C-$CH_4$ profiles 11 km south of the Logatchev hydrothermal field in February (circles, MSM 278) and December 2007 (squares, ATA 20).

14.76°N and 14.78°N the water samples collected during the tow-yo near this depth contained low $^3$He/$^4$He ratios and methane concentrations. This also appears as an "intrusion" of isotopically lighter methane in Figure 2c. The two *L'Atalante* stations north of 14.78°N (ATA22 and ATA18), however, indicate the presence of the upper 2750-m plume north of the hydrothermal field later in the year. Two other *L'Atalante* stations (ATA25 and 28), taken at the same position 2 days apart, intersected the path of the *Merian* tow-yo. These stations, which are about 1.5 km north of the vent field, showed a high degree of variability in the vertical profiles of $\delta^3$He and methane. Methane $\delta^{13}$C values as low as −20‰ found during the tow-yo were absent at this position in the later part of the year (see section 8 below).

[15] The distribution of methane $\delta^{13}$C differs from the patterns exhibited by $\delta^3$He and methane concentration (Figure 2c). In the vicinity of the main vent field, a relatively uniform $\delta^{13}$C of about −13‰ from the bottom upward to a depth of 2400 m reflects the carbon isotope ratio of methane in the vent fluids. Methane with this isotopic ratio also extends southward at 2750-m depth, coincident with the methane plume at that level. Heavier carbon isotope ratios ($\delta^{13}$C > −10‰) developed with distance from the vents, but these ratios were more extensive to the north of the vent field than south of it. To the south at the time of the *Merian* cruise, heavy isotope ratios developed with distance directly underneath the 2750 m plume axis, but not overtop of it. When the southernmost station was reoccupied by *L'Atalante* 11 months later (ATA 20), a methane peak was again found at 2750 m, with a somewhat lower maximum concentration. The carbon isotope ratio of the peak methane had increased significantly, from $\delta^{13}$C = −13‰ to −2‰ (Figure 3), which may be indicative of either more extensive oxidation or a contribution of heavy C isotopes from LHF-2. The carbon isotope ratio of $CH_4$ in LHF-2 vent fluids has been found to be heavier than at LHF-1 [*Charlou et al.*, 2009], but the distribution of the plume from this vent is unknown.

[16] On the five stations where carbon isotopes were measured above 2300 m, the isotope ratio grades toward lighter values upward from this depth (see Figures 7, 9, and 10). The gradient is quite sharp at about 2100 m. Relatively low isotope ratios ($\delta^{13}$C < −14‰) also appeared in low concentrations of methane found in near-bottom water to the south of the vent field (Figure 2c).

## 4. $CH_4$ Versus $\delta^3$He

[17] Measured values of methane concentration in the LHF region are plotted against $\delta^3$He in Figure 4. Most of the measurements are fairly well correlated with a slope corresponding to a $CH_4/^3$He mole ratio of $1 \times 10^8$, which was also observed in the Rainbow hydrothermal plume [*Jean-Baptiste et al.*, 2004]. Such high $CH_4/^3$He ratios may be a characteristic of ultramafic hosted hydrothermal vents. The plume from the "Drachenschlund" at 8° 18′S on the MAR, another high-temperature vent affected by serpentinization, indicates a $CH_4/^3$He ratio of about $4 \times 10^8$ [*Keir et al.*, 2008].

## 5. Mixing With Background Methane

[18] Although the $\delta^{13}$C of background methane throughout the ocean is very poorly known, it is

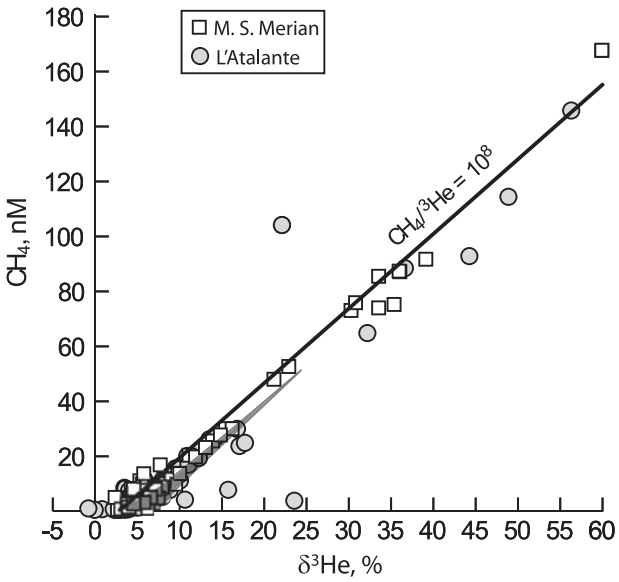


**Figure 4.** $CH_4$ concentration versus $\delta^3$He in the water column at depths > 1800 m from *M. S. Merian* (squares) and *L'Atalante* (circles). Line shows conservative addition of $CH_4$ and $^3$He with a ratio of $10^8$ to a solution containing $\delta^3$He = 3%, [$CH_4$] = 0.5 nM. Methane oxidation in the model results in a $CH_4$ versus $\delta^3$He distribution within the area indicated by the gray shading.

likely to be less than the $\delta^{13}$C of methane from the LHF. For example, *Holmes et al.* [2000] measured values of −35 to −42‰ between 2000 and 4000 m in the central North Pacific. *Cowen et al.* [2002] determined values between −40 and −50‰ at 2000 m in the eastern North Pacific. In newly formed components of North Atlantic Deep Water, methane $\delta^{13}$C varies from −43‰ in Labrador Sea Water at 2000 m depth to −37‰ at 3400 m [*Keir et al.*, 2005]. At a test station 550 km off-axis to the west of the LHF during the *Merian* cruise (MSM 242, see Figure 1a for position), we measured an average $\delta^{13}$C of −35.8 ± 2.7‰ on methane extracted from four water samples (0.7 ± 0.1 nM) collected at 2995 m depth.

[19] Figure 5 shows a plot of methane $\delta^{13}$C versus concentration for all samples collected below 1800 m depth in the LHF region (stations in Figure 1b). Also shown is a mixing line generated by adding methane with $\delta^{13}$C = −13.5‰ to a solution of 0.5 nM $CH_4$ with $\delta^{13}$C = −35‰. The measured carbon isotope ratios either lie on this line or they cluster with higher values above it. The largest deviations from the mixing line occur at the lowest concentrations, at which there exists a wide range of $\delta^{13}$C. This pattern evidently results from the opposing effects of mixing, which tends to produce light isotopic ratios at low concentrations, and consumption, which tends to produce heavy $\delta^{13}$C in the depleted methane.

## 6. Advection-Diffusion Model: Description

[20] We constructed a highly idealized advection-diffusion model in order to observe how mixing and flow together with oxidation affect the relationship of $\delta^3$He, methane concentration and $\delta^{13}$C in a such a system. The model is two-dimensional, consisting of a rectangle 2 km high and 50 km long, which we conceive of as a rift valley segment open at both ends. Horizontal advection is uniform throughout the model space, and there is no vertical advection. Concentration and isotope ratios are fixed at open ocean values at the top boundary, and there is no flux at the bottom. At the entrance (left boundary), influx due to the flow of background water is balanced by the combination of advection and horizontal diffusion away from the boundary. Outflux at the right boundary is carried solely by advection. The model contains a single point source located 9.75 km downstream of the entrance and 900 m below the top boundary. As such the source is 1100 m above the bottom, which is a much greater height than that of plumes ascending from hydrothermal vent fields. However, LHF-1 is situated on a protrusion of the eastern

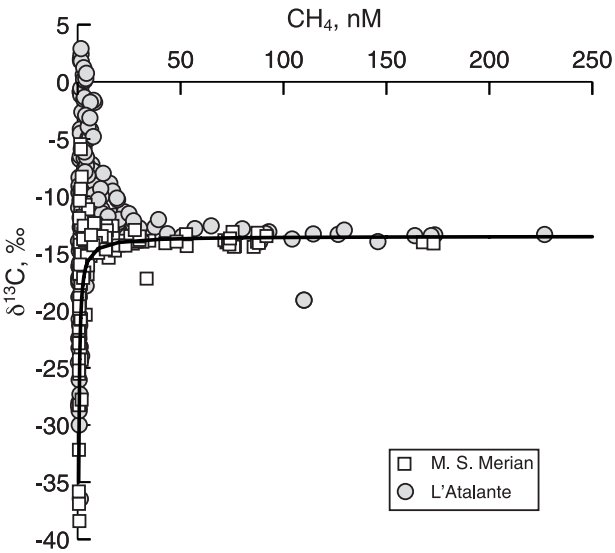


**Figure 5.** Methane $\delta^{13}$C versus concentration for *M.S. Merian* (squares) and *L'Atalante* (circles) samples below 1800 m. Line shows effect of adding methane with $\delta^{13}$C = −13.5‰ to seawater containing 0.5 nM methane with $\delta^{13}$C = −35‰.

wall that is about 800 m above the valley floor. The height of the point source in the model corresponds roughly to that elevation plus the rise height of the plume. The effect of regionally distributed sources (e.g., LHF-2) has not been considered in the model.

[21] As mentioned in the introduction, the oxidation rate of methane appears to depend on bacterial mass and virtually ceases below a certain background methane concentration. *Nihous and Masutani* [2007] take the former into account by including methantroph carbon concentration as a state variable and formulating the consumption kinetics as proportional to the product of it and the methane concentration. In their models, methane is completely consumed at distance from the source. We considered the kinetics in such a way that consumption depends only on the concentration of methane, but it is not completely depleted. The specific oxidation rate is taken to be constant when the resulting $[CH_4] \geq 0.5$ nM. Below this threshold, all reaction ceases. Above this threshold, the ratio of the rate constants for $^{12}CH_4$ and $^{13}CH_4$ oxidation, $^{12}k_{ox}$ and $^{13}k_{ox}$, is also assumed to be constant with an isotope fractionation factor, $\alpha = {}^{12}k_{ox}/{}^{13}k_{ox}$. Because of the discontinuity in the kinetics, there exists a region surrounding the source in which oxidization takes place and the methane concentration remains above or equal to the threshold. The method used for finding this region during the numerical solution of the methane distribution is described in Appendix A.

[22] An important reason for the inclusion of the kinetic discontinuity is that it adds a certain amount of "realism" to the distribution of carbon isotope ratios. Methane advecting or diffusing into the model only begins to be consumed when higher concentrations dispersing from the source are encountered. Thus, carbon isotope ratios within the model space containing background methane levels are not subject to fractionation locally. With continuous first-order kinetics on the other hand, methane begins to decrease on entering the model space, and because of isotope fractionation, very low concentrations of methane containing high $\delta^{13}C$ develop upstream, away from the source. This has not been observed in the field.

[23] Helium-3 in the model was calculated by treating the $^3He/^4He$ ratio as a mass conserving tracer. This would be strictly true only if the $^4He$ concentration remained constant, which it does not. However, this is a reasonably good approximation over the range of $\delta^3He$ values simulated, 3–24%. Assuming a background $^4He$ concentration of 1.9 nM and a $^3He/^4He$ source ratio of $10^{-5}$ (7 $R_{atm}$) [*Jean-Baptiste et al.*, 2004], a $\delta^3He$ increase of 21% corresponds to a $^4He$ increase of 0.068 nM, which is 3.6% of the background concentration.

## 7. Model Parameterization

[24] The physical parameters of the model were chosen on the basis of work done in other rift valley segments on the MAR. These are as follows:

[25] 1. Horizontal advection, $u$ = 100 km $a^{-1} \approx$ 0.3 cm $s^{-1}$. Thus, the residence time of water in the model is 0.5 year. *Murton et al.* [1999] estimate a replacement time of 0.7 years in the Broken Spur segment; *Thurnherr et al.* [2002] estimate water residence times of 3 and 5 months in the AMAR and South AMAR segments near 36°N.

[26] 2. Vertical eddy diffusion, $K_z$ = 0.3 $km^2$ $a^{-1} \approx$ 0.01 $m^2$ $s^{-1}$. This value is greater than found on the flanks of the MAR [*Polzin et al.*, 1997], but it is the same order of magnitude as $K_z$ found by *Thurnherr* [2006] in the rift valley at 36°N. This vertical eddy diffusion is also similar to estimates of $K_z$ in the vicinity of the Drachenschlund hydrothermal vent based on methane distribution [*Keir et al.*, 2008] and on density profiles from tow-yo CTD casts (M. Walter et al., Rapid dispersal of a hydrothermal plume by turbulent mixing, submitted to *Deep Sea Research*, 2009).

[27] 3. Horizontal eddy diffusion, $K_x$ = 300 $km^2$ $a^{-1} \approx$ 10 $m^2$ $s^{-1}$. This is a guess at what may be a crude analog of dispersion in the presence of tidally varying currents. Lateral dispersion of the methane plume from the Drachenschlund vent appeared to be in the range of 2–20 $m^2$ $s^{-1}$ [*Keir et al.*, 2008]. The $K_x$ we employ in the model is greater than what one might expect in the surface ocean, where horizontal eddy diffusion appears to be dependent on the length scale of mixing [*Joseph and Sendner*, 1958]. According to *Okubo*'s [1971] summary of tracer release experiments, a $K_x$ of 0.3 $m^2$ $s^{-1}$ would be expected for a 50 km length scale.

[28] The chemical parameters in the model were chosen somewhat arbitrarily and not so much with the intention of fitting the model to the data that we collected. The rate constant for methane oxidation at concentrations $\geq$0.5 nM, $k_{ox}$ = 10 $a^{-1}$, is a rough average of results obtained from previous plume studies [*de Angelis et al.*, 1993; *Tsunogai et al.*,

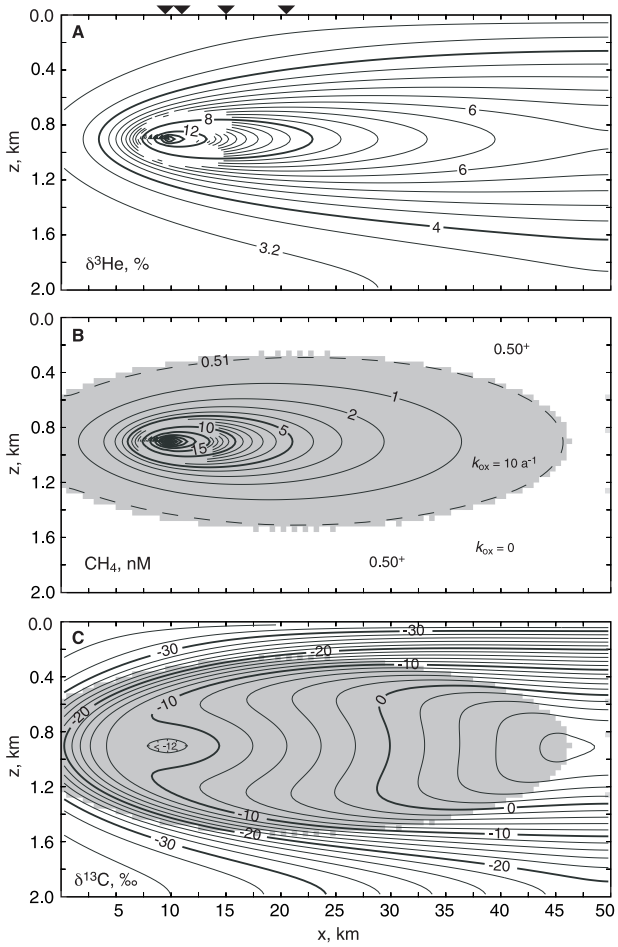


**Figure 6.** Model-simulated sections of (a) $\delta^3$He, (b) $CH_4$ concentration, and (c) $\delta^{13}$C-$CH_4$. In Figures 6b and 6c, $CH_4$ consumption in the gray area is first-order with $k_{ox} = 10\ a^{-1}$; outside of this region (white area), $k_{ox} = 0$. In Figure 6c, the isotope fractionation factor $\alpha = 1.010$ within the gray area. Markers at top indicate x position of vertical model profiles shown in Figures 7–10.

2000; *Valentine et al.*, 2001; *Grant and Whiticar*, 2002; *Keir et al.*, 2008]. The isotope fractionation factor in the model is taken for illustrative purposes to be $\alpha = 1.010$, which is within the range of previous studies [*Tsunogai et al.*, 2000; *Grant and Whiticar*, 2002; *Heeschen et al.*, 2004; *Kinnaman et al.*, 2007]. The molar ratio of $CH_4$ to $^3$He in the model source is $10^8$, which is what is observed at LHF-1. A methane flux per unit width equal to 1000 mol $m^{-1}$ $a^{-1}$ was supplied to the 40 m × 500 m box enclosing the source. This source produces a $CH_4$ maximum of about 50 nM within this grid box, which is well above background but not necessarily typical of the water column within a few hundred meters of the LHF-1 vents. Higher concentrations were often encountered in this vicinity during the *Merian* and *L'Atalante* cruises, especially during tow-yos over the vent field. The $\delta^{13}$C of the methane source was taken as −14‰, the original value measured by *Lein et al.* [2000].

## 8. Model Results

[29] The distributions of $\delta^3$He, methane and methane $\delta^{13}$C produced by the model are shown in Figure 6. The shape of the $^3$He and methane plumes appear similar near the source, e.g., in the region where $\delta^3$He > 8% and [$CH_4$] > 5 nM. Methane is determined by the model kinetics to be consumed within the gray area shown in Figures 6b and 6c. Outside of this area, $k_{ox} = 0$, and the resulting methane concentrations in this area are nearly constant with a mean of 0.503 ± 0.002 nM.

[30] Methane $\delta^{13}$C (Figure 6c) has a different shape distribution than those of $\delta^3$He and methane concentration. Heavy values develop progressively downstream in the plume because of isotope fractionation. At the depth of the source, this continues until methane oxidation ceases, at which point the maximum $\delta^{13}$C is reached. At any particular position downstream of the source, a broad vertical interval of relatively constant $\delta^{13}$C develops that is bounded above and below by sharp vertical gradients toward lighter values. The isotope ratio of high concentrations of methane is nearly unaffected by mixing with lighter methane at low concentration, and near the source, consumption and isotope fractionation increase the $^{13}$C/$^{12}$C ratio as methane mixes vertically. This produces a slight double maximum in the $\delta^{13}$C vertical profile. Farther out on the flanks of the plume where methane decreases to levels approaching that of the background, mixing with low-$\delta^{13}$C, low-concentration methane reverses this trend and sharp gradients occur.

[31] In Figure 4 the domain of model-predicted $CH_4$ versus $\delta^3$He (gray transparency) is superimposed on the measured data. Oxidation in the model perturbs the mixing line such that these properties occupy a narrow triangular-shaped area below the line. Higher concentrations of $CH_4$ and $^3$He extend parallel to the mixing line, while the lowest methane concentrations in the model are associated with a range of $\delta^3$He between 3% (the low end-member) and 7%. This pattern seems to appear in the data as well, with the observed $\delta^3$He at low $CH_4$ concentrations scattered over a somewhat broader range. Besides measurement deviations, this

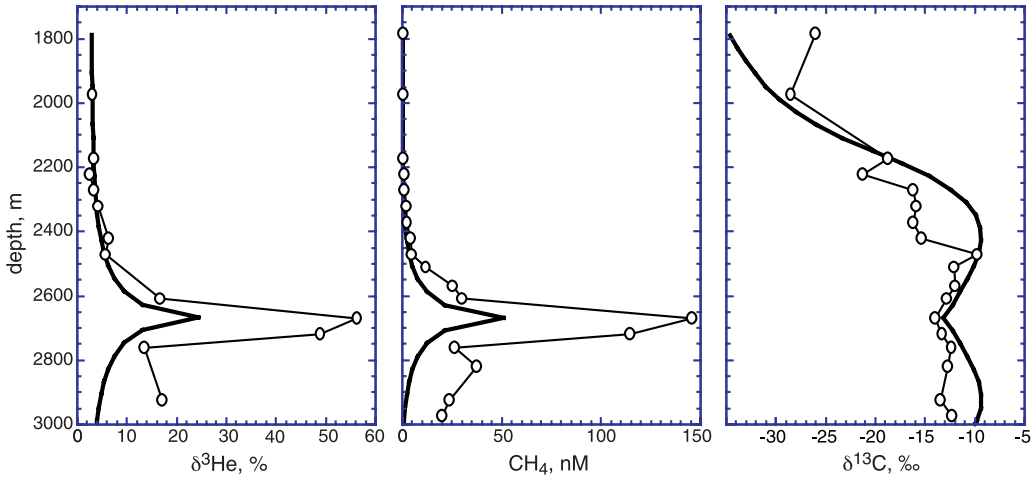


**Figure 7.** Profiles of $\delta^3$He, $CH_4$ concentration, and $\delta^{13}$C-$CH_4$ 100 m north of LHF-1 vent field (*L'Atalante* Station 10). Bold line shows calculated profiles at source position (x = 9.5 km) in the model.

may be due to variation of background $^3$He with depth outside the rift valley (see section 10 below), which is not considered in the model.

## 9. Vertical Distribution of Tracers in the Hydrothermal Plume and in the Model

[32] To the north of LHF-1, the measured tracer profiles resemble to some degree those simulated at the corresponding distance downstream of the source by the model (Figures 7–10). Maximum concentrations of $^3$He and $CH_4$ at ATA-10 near the vent field are 2 to 3 times higher than those simulated by the model at the source position (Figure 7), but the concentration profiles beyond 5 km downstream become more similar to those observed (Figures 9 and 10). In contrast to the concentrations, the model-simulated $\delta^{13}$C-$CH_4$ profiles are fairly similar to those observed at all four station positions north of LHF-1 (Figures 7–10). We regard the above discrepancy as a limitation of the 2-D model in which the plume cannot disperse as rapidly as in the three-dimensional ocean where lateral dispersion normal to the plume axis also occurs. This limitation does not seem to manifest itself clearly on the methane $^{13}$C/$^{12}$C ratios because mixing only affects them as low

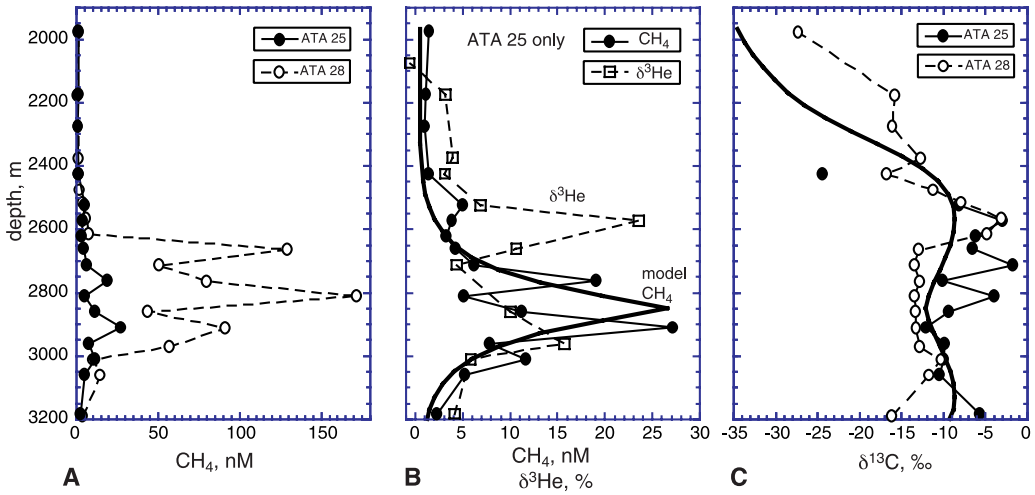


**Figure 8.** Profiles of $\delta^3$He, $CH_4$ concentration, and $\delta^{13}$C-$CH_4$ 1.5 km north of Logatchev field: (a) $CH_4$ concentration profiles from *L'Atalante* stations 25 (filled ovals) and 28 (open ovals), (b) $CH_4$ concentration (ovals) and $\delta^3$He (squares) from Station 25 only, and (c) $\delta^{13}$C-$CH_4$ from stations 25 (filled ovals) and 28 (open ovals). Heavy lines indicate model-simulated profiles of $CH_4$ in Figure 8b and $\delta^{13}$C-$CH_4$ in Figure 8c, at a position 1.5 km downstream of source (x = 11 km).

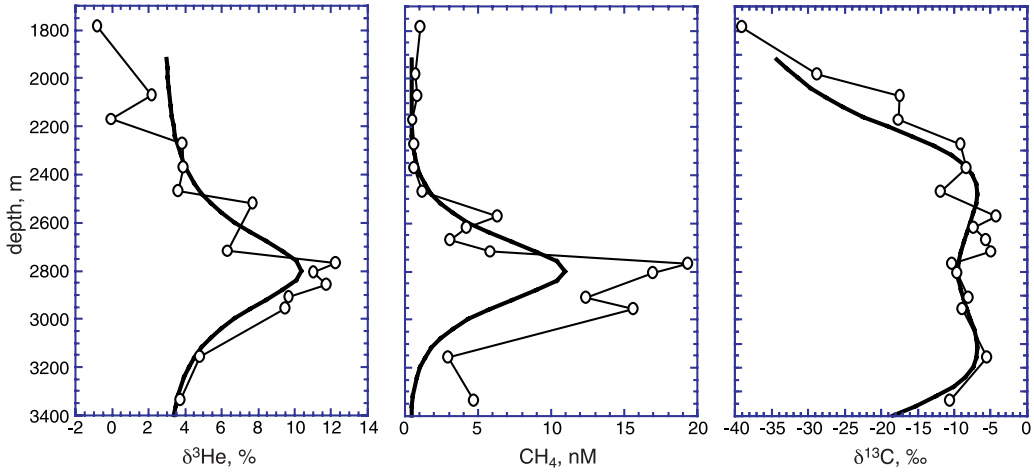


**Figure 9.** Profiles of $\delta^3$He, $CH_4$ concentration, and $\delta^{13}$C-$CH_4$ 5.5 km north of Logatchev field (*L'Atalante* Station 22, ovals). Heavy lines show model-produced profiles 5.5 km downstream of source (x = 15 km).

concentrations are approached. For example, whether the methane concentration at the source position is 100 × or 300 × the background has no significant effect on the isotope ratio.

[33] Temporal variation of tracers near the vent field can be large, as seen at two stations (ATA 25 and 28) 1.5 km north of the vent field that were taken 2 days apart. The maximum methane concentration increased by a factor of about 6 during this time (Figure 8a), while $\delta^{13}$C shows a small decrease (Figure 8c). This may be expected since intrusion of "fresh" hydrothermal methane should decrease the $\delta^{13}$C toward a limit of about −13‰. The measured profiles of methane and $\delta^3$He are "noisy" with multiple peaks. Helium isotopes were only measured on ATA Station 25, and here a strong peak of $\delta^3$He that had no methane counterpart occurred at 2570 m (Figure 8b). At this depth on both stations, the methane $\delta^{13}$C exhibits a positive excursion to about −3‰, perhaps indicating enhanced microbial oxidation at this depth (Figure 8c).

[34] During the *L'Atalante* cruise, the most distant stations were taken 11 km from the hydrothermal field, to the north (ATA 18), south (ATA 20), and west (ATA 11; positions in Figure 1b). Maximum concentrations of methane and $^3$He were somewhat different at these stations, with lower values to the

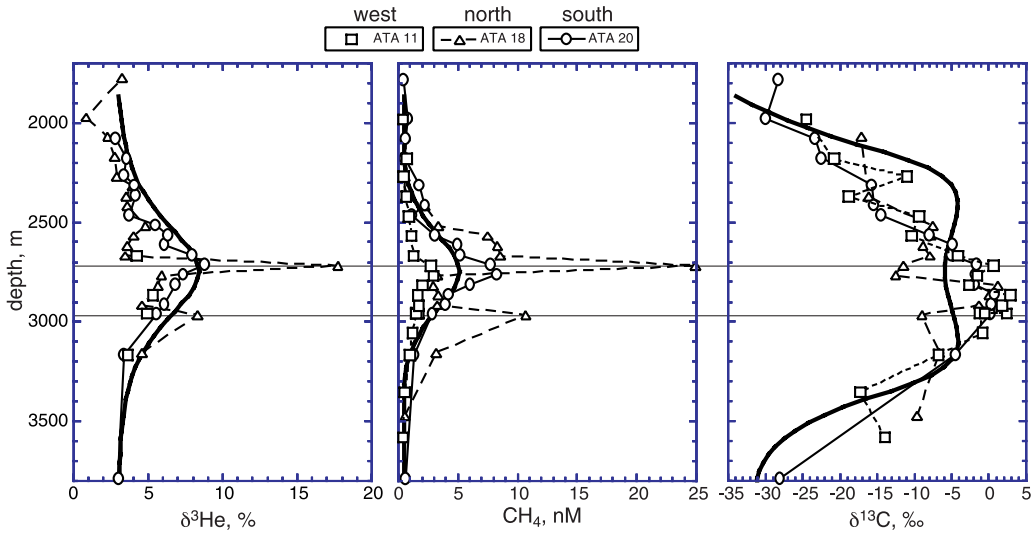


**Figure 10.** Profiles of $\delta^3$He, $CH_4$ concentration, and $\delta^{13}$C-$CH_4$ 11 km to the south (ovals, ATA 20), north (triangles, ATA 18), and west (squares, ATA 11) of the Logatchev field. Heavy lines show model-produced profiles 11 km downstream of the source (x = 20.5 km). Horizontal lines mark depths of $\delta^3$He and $CH_4$ "spikes."

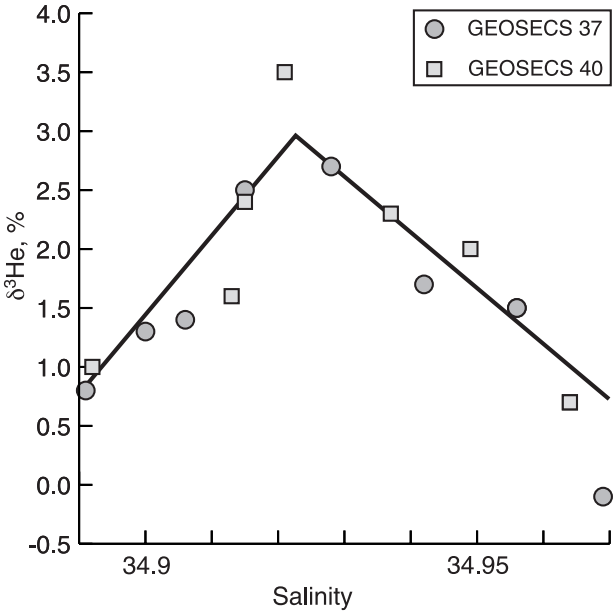


**Figure 11.** Salinity versus $\delta^3$He at GEOSECS stations 37 (circles) and 40 (squares), in the depth interval between 2000 and 4000 m (data from *Jenkins and Clarke* [1976]). Line shows function used to derive background $\delta^3He_0$ values for calculating methane concentration expected in the absence of mixing (equation (1)).

west, but the $\delta^{13}$C profiles were fairly similar at all three (Figure 10). These stations exhibit the heaviest carbon isotope ratios, which reach a $\delta^{13}$C of about +2‰. Although conceptually all 3 stations cannot be "downstream" at the same time, there is a certain similarity between these station profiles and those produced by the model 11 km downstream of the source. At ATA 18 (north), the methane and $\delta^3$He profiles contain spikes at 2710 and 2980 m. At these depths, the methane $\delta^{13}$C shows negative excursions toward the vent fluid value, as if layers of hydrothermal methane were intruding into the aging plume.

[35] The overall similarity of the tracer distributions predicted by the model to those observed north of LHF-1 may indicate that, despite the complicated mixing and circulation within the rift valley, the model serves as a rough analog of the interaction of mixing and isotope fractionation within the system.

## 10. Kinetic Isotope Fractionation Factor

[36] In order to estimate the kinetic isotope fractionation, we first consider the methane concentration and $\delta^{13}$C that would result from mixing vent fluid with background seawater in the absence of oxidation. Since helium is a conservative tracer, the increase of $\delta^3$He over its background value, $\delta^3He_0$,

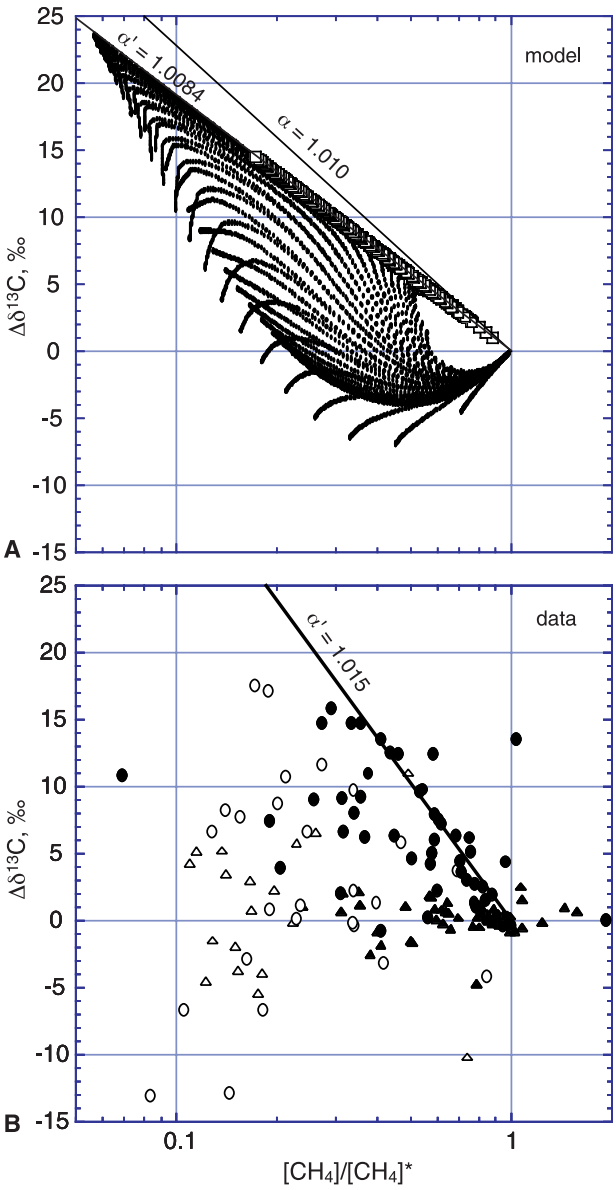


**Figure 12.** Deviation of methane $\delta^{13}$C from value expected from mixing only ($\Delta\delta^{13}$C) versus ratio of "observed" to expected $CH_4$ concentration ($[CH_4]/[CH_4]^*$). (a) Model result: squares indicate $[CH_4] \geq 2$ nM, and other points correspond to $[CH_4] < 2$ nM. Lines indicate closed system trends for the input isotope fractionation factor ($\alpha = 1.010$) and the apparent factor ($\alpha' = 1.0084$) "derived" from upper boundary of scatterplot. (b) $\Delta\delta^{13}$C versus $[CH_4]/[CH_4]^*$ from *Merian* 4/3 (triangles) and *L'Atalante* (ovals) data. Solid points correspond to $[CH_4] \geq 2$ nM. Line indicates $\alpha'$ that appears to be approximate upper bound to the scatterplot.

**Table 2.** Comparison of $[CH_4]$ and $CH_4$-$\delta^{13}C$ Corresponding to $\delta^3He$ = 3.225% Under Various Circumstances of Mixing With Background Water and Oxidation With $\alpha$ = 1.01

| Conditions | $[CH_4]$ (nM) | $\delta^{13}C$ (‰) |
|---|---|---|
| Mixing only, no oxidation | 1.11 | −23.46 |
| Mixing first, then closed system oxidation | 0.50 | −15.73 |
| Oxidation first,[a] following by mixing | 0.50 | −34.28 |
| Model at x = 49.75 km, z = 60 m | 0.50 | −30.42 |

[a] Ninety-nine percent consumption of $CH_4$ at source position (x = 9.75 km, z = 900 m) containing $\delta^3He$ = 24.42%, $[CH_4]$ = 51.48 nM, $\delta^{13}C$ = −13.16‰.

should indicate the amount of hydrothermal methane that would be added to a parcel of seawater in the absence of consumption. A problem here is that the background level of $\delta^3He_0$ is not perfectly constant throughout the depth range of the rift valley (2–4 km). In the western tropical Atlantic (GEOSECS stations 37 and 40; positions in Figure 1a), there is a small $\delta^3He$ maximum of about 3% at 3 km depth and minimum values of about 1% above and below at 2 and 4 km depth [*Jenkins and Clarke*, 1976]. Salinity at these stations decreases continuously from 34.97 to 34.89 psu throughout this depth range. On this basis, we use the measured sample salinity to assign $\delta^3He_0$ using the function shown in Figure 11. From the trend of $CH_4$ versus $\delta^3He$ at high concentrations, the methane concentration expected in the absence of oxidation, $C^*$, is calculated from

$$C^*_{CH4} = 0.5 + 2.714\left(\delta^3He - \delta^3He_0\right), \quad (1)$$

where the slope corresponds to a $CH_4/^3He$ mole ratio of $10^8$ in the vent source. The carbon isotope ratio expected in the absence of oxidation, $\delta^*$, can then be calculated from the mixing equation

$$\delta^* = \delta_p - \frac{C_0}{C^*}\left(\delta_p - \delta_0\right), \quad (2)$$

where $\delta_p$ refers to the $\delta^{13}C$ of methane in the vent fluid, and the subscript, 0, refers to methane concentration and $\delta^{13}C$ in background seawater, taken as 0.5 nM and −35‰. The fraction of methane remaining after subsequent oxidation can then be calculated as $f = C_{CH4}/C^*_{CH4}$, where $C_{CH4}$ is the measured or the model-simulated concentration. The apparent increase in the carbon isotope ratio, $\Delta\delta^{13}C$, can be obtained from the difference between the observed $\delta^{13}C$ and that expected from mixing only in equation (2).

[37] If the vent fluid first mixed rapidly with background seawater within a certain volume of the plume and this were followed by oxidation in a closed system as this volume "aged," one would expect $\Delta\delta^{13}C$ to follow the Rayleigh relationship given by

$$\Delta\delta^{13}C \cong \left(\frac{1}{\alpha} - 1\right)\ln f \quad (3)$$

The remaining fraction, $f$, and $\Delta\delta^{13}C$ have been calculated from the model results and from the observed data according to the procedure above and plotted in the diagrams shown in Figure 12. In neither case do the entire data/model sets follow a linear relationship (on a semilog plot) as predicted from equation (3). In the case of the model, many of the points, including all of those where $[CH_4] \geq$ 2 nM (squares in Figure 12a), fall on a straight line that forms an upper limit of $\Delta\delta^{13}C$ at any particular $f$ (Figure 12a). The slope of this line is equivalent to a fractionation factor (1.0084) that is slightly less than the value ($\alpha$ = 1.010) applied in the model. This deviation from the true value appears to occur because the system is open to mixing with methane in background water with relatively low $\delta^{13}C$. $\Delta\delta^{13}C$ values less than predicted by the apparent fractionation factor occur in the "far-field" away from the source, in low concentrations of methane. The diagram of $\Delta\delta^{13}C$ versus log $f$ derived from the measured data also appears as a cloud of points bounded by a negative sloping line (Figure 12b). Almost all data that fall on or near this line come from *L'Atalante* samples with $[CH_4] \geq$ 2 nM, but in contrast to the model, not all data with $[CH_4] \geq$ 2 nM fall on the line.

[38] The $\Delta\delta^{13}C$ values that are lower than expected from the Rayleigh function indicate that mixing is not rapid compared to oxidation throughout the entire rift valley/model domain. Even negative $\Delta\delta^{13}C$ values appear, both in the model and the data, which means that oxidation has resulted in lower methane $\delta^{13}C$ at that particular location than the isotope ratio would have been in the absence of consumption. This may at first seem strange. Negative $\Delta\delta^{13}C$ occur on the outer flanks of the model plume, where the hydrothermal methane component has already strongly decreased because of prior consumption before reaching these locations. This reduces the percentage of hydrothermal source methane (but not $^3He$) mixing with background water to such an extent that the resulting $\delta^{13}C$ is less than it otherwise would have been if the nonoxidized aliquot of hydrothermal methane

with $\delta^{13}C = -14‰$ had been allowed to mix to this point. This may be illustrated by the following example.

[39] In the model, the most negative $\Delta\delta^{13}C = -6.96‰$ occurs far downstream near the top and right boundaries (x = 49.75 km, z = 60 m). $\delta^3He = 3.225\%$ at this position, from which $C^*_{CH4}$ in the absence of oxidation is found from equation (1) to be 1.1105 nM. From equation (2), $\delta^{13}C^*$ is calculated to be $-23.46‰$. (These values are also found when the model is run with $k_{ox} = 0$). If 55% of this methane were then consumed in a closed system with $\alpha = 1.01$, a concentration of 0.5 nM and $\delta^{13}C$ of $-15.71‰$ would result. However, the model produces $C_{CH4} = 0.50$ nM and $\delta^{13}C = -30.42‰$ at this position, the latter being lower than even the $\delta^{13}C^*$ calculated in the absence of oxidation. Alternatively, we can consider an initial rapid oxidation of methane starting with the tracer values in the grid box surrounding the source (x = 9.75 km, z = 900 m), which are $\delta^3He = 24.42\%$, $C_{CH4} = 51.48$ nM and $\delta^{13}C = -13.16‰$. If about 99% of this methane were first consumed in a closed volume as it moved downstream, a concentration of 0.5 nM would be achieved, and $\delta^{13}C$ would increase to +33.13‰ according to equation (3). The $\delta^3He$ (3.225%) at x = 49.75, z = 60 would be achieved by mixing 1.05% of this "predepleted" water with 98.95% background water containing $\delta^3He = 3\%$. The methane concentration of this mixture would still be 0.50 nM, and the methane $\delta^{13}C$ would be $[0.0105 \times (+33.13) + 0.9895 \times (-35)] = -34.28‰$. Thus, despite its large increase in $\delta^{13}C$, the hydrothermal methane component in this scenario becomes too small to appreciably affect the carbon isotope ratio. Thus, the "order of events," the relative rates of mixing and consumption, as the plume ages can make a big difference in the resulting carbon isotope ratio. Because of its distance from the source and its proximity to the upper boundary, the model-simulated $\delta^{13}C$ at x = 49.75, z = 60 is more similar to the "oxidation-first" extreme than to that of "mixing-first." These cases are summarized in Table 2.

[40] The similarities between observed and model-produced vertical profiles shown in the previous section suggest that the LHF plumes behave somewhat analogously to the model. Since "elevated" concentrations ($\geq$2 nM) of methane seem to behave roughly analogous to locally rapid mixing in the near-field, we interpret the "boundary" line in Figure 12b as indicating the approximate value of the fractionation factor. The apparent value of $\alpha$ corresponding to the slope of this line is 1.015. If our model analog is correct, the true value of $\alpha$ might be a little higher because of the effect of hydrothermal methane depletion.

## 11. Discussion

[41] As mentioned in the introduction, a few studies have found low isotope fractionation factors in the deep sea, with $\alpha$ on the order of 1.004 to 1.008 [*Tsunogai et al.*, 2000; *Cowen et al.*, 2002; *Heeschen et al.*, 2004]. Considering that the neutrally buoyant plumes from the LHF have roughly similar temperatures, between 2 to 3°C, to environmental conditions in those studies, the fractionation factor that we obtain appears somewhat higher. On the other hand, the isotope fractionation that we find is less than observed in the laboratory experiments of *Kinnaman et al.* [2007], who report an $\alpha = 1.027 \pm 0.004$ from incubations of sediment obtained at cold seeps. This could be due, at least in part, to the warmer temperature (15°C) of their experiments. *Kinnaman et al.* [2007] also found that the methane carbon isotope fractionation appeared to change during the course of the incubations, with lower fractionation occurring near the end of the experiments. They suggest that this might have been caused by substrate limitation being reached at the relatively lower methane concentrations. Thus, qualitatively, one might expect that fractionation might be greater in environments with relatively higher methane concentrations. LHF-1 is certainly one of those areas, with methane concentrations up to about 500 nM in samples collected on tow-yo CTDs over the site. The maximum methane concentrations at the sites studied by *Tsunogai et al.* [2000] (Myojin Knoll Caldera) and *Heeschen et al.* [2004] (Weddell Sea Bottom Water) are significantly lower (12 nM and 3 nM respectively). These workers found the lowest fractionation factors of about 1.005. In contrast, the Endeavor Segment of the Juan de Fuca Ridge produces a powerful methane plume supplied by thermogenesis [*Lilley et al.*, 1993]. Concentrations up to 600 nM in the plume there were reported in the study of *Cowen et al.* [2002]. Their value of $\alpha = 1.008$ is slightly higher than the fractionation factors found in the Myojin Knoll and in Weddell Sea Bottom Water, but this value is somewhat lower than our estimate for the LHF. Thus, it remains unclear as to what exactly could be promoting variation in carbon isotope fractionation

during microbial consumption of methane in the deep sea.

## 12. Conclusions

[42] The methane geochemistry of the LHF-1 plumes appears to be influenced by advection and mixing of background seawater with vent fluids along with oxidation. Other active sites near the main field, such as LHF-2, may also exert an influence as well. The relationship of methane $\delta^{13}C$ to concentration thereby becomes more complex than in a simple closed system. A model simulation indicates approximate Rayleigh-type fractionation can appear in the near field plume where mixing occurs on a shorter time scale than that of methane oxidation. Applying this analogy to the Logatchev plume data, it appears that the kinetic fractionation factor is about 1.015. The model and the observations also indicate that the relative rates of consumption and mixing with background seawater as the plume ages exerts a strong influence on the $^{13}C/^{12}C$ ratio of low methane concentrations within the rift valley.

## Appendix A: Calculation of Rate Constant Matrix and Methane Distribution

[43] The model distribution of the methane concentration, $q(x, z)$, is governed by the partial differential equation

$$K_x \frac{\partial^2 q}{\partial x^2} + K_z \frac{\partial^2 q}{\partial z^2} - u \frac{\partial q}{\partial x} - k(q)q + J(x,z) = 0, \qquad \text{(A1)}$$

where the physical parameters, $u$, $K_x$ and $K_z$ are taken to be constant throughout the model domain. There is a point source, $J(a, b) = J_0$; otherwise $J(x, z) = 0$. The methane concentration at the top boundary is fixed at a "background" concentration, $c_b$. Methane with this concentration advects into the model domain at the left boundary, and at the right boundary ($x = L_1$), all of the outflux is carried by the flow. At the bottom ($z = L_2$), there is no flux. Formally, the boundary conditions are as follows:

$$q = c_b \text{ at } z = 0,$$
$$dq/dz = 0 \text{ at } z = L_2$$
$$-K_x \left.\frac{dq}{dx}\right|_{x=0^+} + uq = uc_b \text{ at } x = 0$$
$$dq/dx = 0 \text{ at } x = L_1.$$

[44] The specific rate of methane consumption, $k(q)$, is two-valued, being either a specified constant, $k_1$, or zero. Which value applies at a particular point (x, z) is determined by whether or not $q(x, z) < c_b$ results at this point when $k(x, z) = k_1$. If this is true, then $k(x, z) = 0$; otherwise $k(x, z) = k_1$. One could think of this as "sufficient or starve" consumption. Either there is a supply of methane $\geq k_1\ c_b$ to a particular position, in which case the consumption is first-order, or otherwise there is no consumption at that position. Thus, the problem is to find both the methane distribution that satisfies equation (1) and the associated $k(x, z)$ that satisfies the "sufficient or starve" condition.

[45] We attempted to solve this problem with a numerical approach. Equation (1) is replaced with a set of five-point finite difference equations in which the distribution is represented by $M \times N$ grid cells of size $h_1 \times h_2$ in the horizontal and vertical directions, where $h_1 = L_1/M$ and $h_2 = L_2/N$. Defining the ratios, $r_1 = u/h_1$, $r_2 = K_x/h_1^2$, $r_3 = K_z/h_2^2$, the difference equation used at an interior point is,

$$[r_1 + 2(r_2 + r_3) + k(x,z)]q(x,y) - (r_1 + r_2)q(x - h_1, z) - r_2 q(x + h_1, z) - r_3[q(x, z - h_2) + q(x, z + h_2)] = J(x,z) \qquad \text{(A2)}$$

[46] A variation of the line iteration method is then used to find both $q(x, z)$ and $k(x, z)$. Horizontal lines were used, and so the last term on the left side of equation (A1) is added to the right. The "off-line" concentrations in brackets, $q(x, z - h_2)$ and $q(x, z + h_2)$ are input from their previously calculated lines. In this way each horizontal line of grid cells represents a system of equations with a tridiagonal matrix of the form

$$B_1 T_1 + C_1 T_2 = D_1$$
$$A_i T_{i-1} + B_i T_i + C_i T_{i+1} = D_i, \ i = 2, 3, \ldots, M - 1 \qquad \text{(A3)}$$
$$A_M T_{M-1} + B_M T_M = D_i$$

where $T_i$ represents the methane concentrations on a particular line with $M$ intervals of $h_1$.

[47] This system can be solved with a well-known algorithm [e.g., *Young and Gregory*, 1973]. In this system, only the diagonal $B_i$ coefficients contain $k_i$. the specific rate in each cell on the horizontal line. Normally, $B_i$ is known and each line of concentrations is solved once, one after another, until the entire domain has been "swept." In our procedure, each iteration consists of repeatedly solving each line, before moving to the next, until a distribution

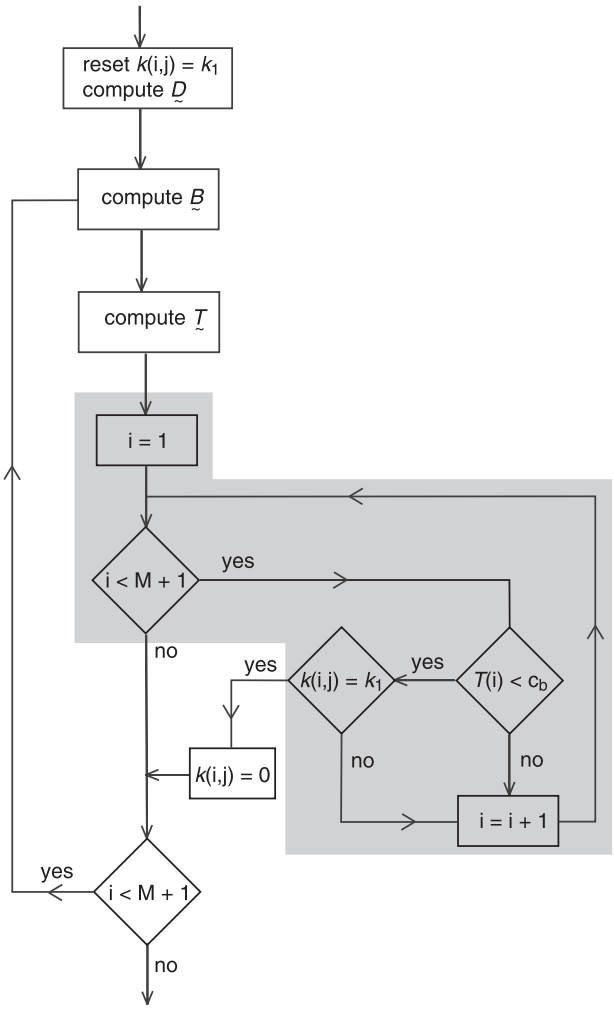


**Figure A1.** Flow diagram of procedure used to determine $k$(i,j) on line $j$ during the line iteration. The gray region is a conventional for-next loop that will be exited with the current $i$ value in the case that the current $k$(i,j) is changed from $k_1$ to 0.

of $k_i = \{0, k_1\}$ has been found that satisfies the "sufficient or starve" criterion above. Then the sweep continues with the next line. This is done in the following way:

[48] 1. On beginning a new line, the $k_i$ from $i = 1$ to M are set to $k_1$, and the $D_i$ coefficients are calculated.

[49] 2. The line of concentrations, $T_i$, is then solved for.

[50] 3. Proceeding from $i = 1$ to $M$, each $T_i$ is checked to see if $T_i < c_b$. When this is found to be true, then the rate constant at that point is checked to see if $k_i = k_1$. If this is also true, then $k_i$ at the current value of $i$ is set to zero and the line of concentrations is recalculated (step 2). If these conditions are not met, then $k_i$ is not altered and the next concentration at $i = i + 1$ is checked.

[51] A flow diagram of this procedure is illustrated in Figure A1. The shaded portion consists of a for-next loop in BASIC that tests each of the concentrations. If at a given $T_i$, both criteria are met, then $k_i$ is set to zero and the for-next loop is exited. A loop-while statement then returns the program to recalculate $B_i$ and solve for $T_i$ again.

[52] This procedure appears to work, but it requires attention since the system does not completely converge to a unique set of $k$(i, j). Instead, one reaches a point where most of the $k$(i, j) remain unchanged from iteration to iteration, but a small number of the $k$(i, j) "flicker," with about an equal number turning off and the other half on during any given iteration (Figure A2). In the computation in this work, there are 5000 cells on a 100 × 50 grid. After 90 iterations, about 99% of $k$(i, j) in these cells remain steady. This region is shown by the white ($k$(i, j) = 0) and gray ($k$(i, j) = 10 $a^{-1}$) areas in Figure A3. $k$(i, j) changes in the remaining 57 cells (colored in Figure A3), about 34 at a time during each iteration, with about half of these $k_{i,j}$ turning on and the other half turning off. Most of these grid cells lie on the boundary between consumption and no consumption; a few additional cells are located at the right boundary of the model. Some of the $k_{i,j}$ on the edge of the consumption region change back

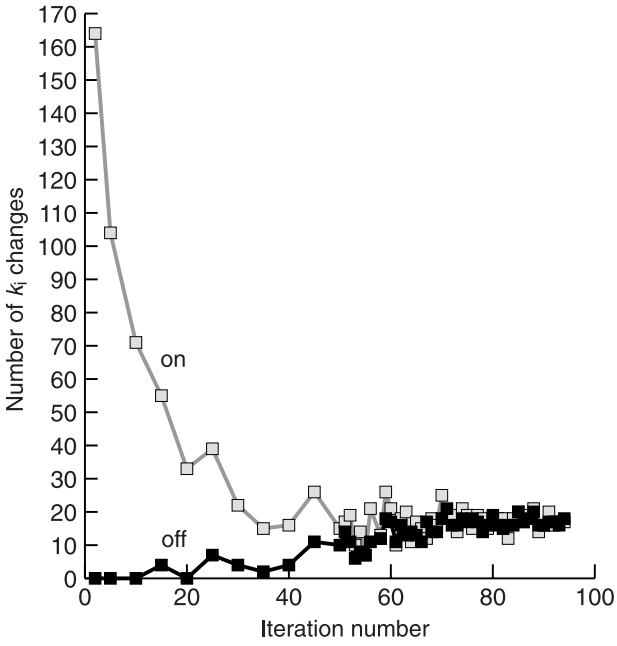


**Figure A2.** The number of $k$(i,j) changing from 0 to 10 $a^{-1}$ ("on," gray points) and from 10 $a^{-1}$ to 0 ("off," black squares) on each iteration.

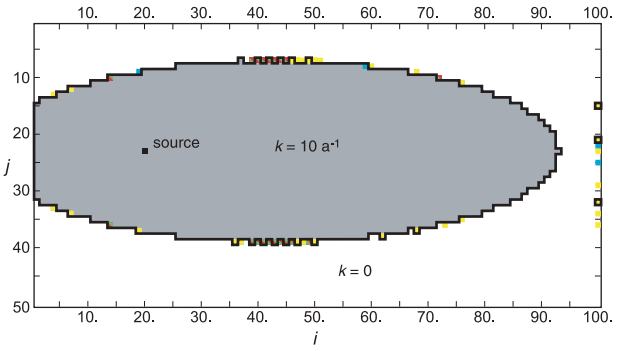


**Figure A3.** Distribution of specific rate, $k$(i,j) values in model domain following after 89 iterations. Gray [$k$(i,j) = 10 $a^{-1}$] and white [$k$(i,j) = 0] areas remain unchanged thereafter. The remaining cells change during iterations 90–94, either frequently (red-green), occasionally (yellow), or infrequently (blue). Lines enclose areas with $k$(i,j) = 10 $a^{-1}$ after the 91st iteration. This $k$(i,j) distribution was fixed and used to determine steady state $CH_4$ and $\delta^{13}C$ distributions.

and forth on almost every iteration. The other grid cells change less frequently. The distributions of methane concentration and $\delta^{13}C$ produced by any particular matrix of $k$ values after the 90th iteration are very nearly the same. Thus, there appears not to be a unique solution but instead a set of nearly identical areal distributions of the digital $k$ values that satisfies the discontinuous rate criteria. Because of the "flickering" $k$(i, j), $q(x, z)$ also does not completely converge during this procedure. Convergence of the methane distribution is achieved by fixing $\boldsymbol{k}$ at some point after the on versus off changes come into balance and then continuing the line iteration until $\boldsymbol{q}$ converges. The changes in $q(x, z)$ during this final relaxation are small, but it is necessary to execute this step if the distribution of carbon isotope ratios is to be subsequently calculated. The results we present were obtained by beginning with 91 iterations using the above procedure. The resulting area of the model that contains $k_{i,j}$ = 10 $a^{-1}$ is outlined in Figure A3 (and shown in gray in Figure 6). The steady methane distribution was obtained after an additional 300 iterations with $\boldsymbol{k}$ held constant.

[53] The same matrix of $k_{i,j}$ values is then applied to computing the distribution of the methane carbon isotopic ratio. First, the rate constant matrix as determined above is replaced by $^{13}\boldsymbol{k} = \boldsymbol{k}/\alpha$, where $\alpha$ is the isotope fractionation factor. The dependent variable in equation (A1) is taken to be $^{13}q = q\,(1 + \delta^{13}C)$, a quantity proportional to [$^{13}CH_4$]. Thus, the source is $^{13}J_0(a, b) = J_0\,(1 + \delta^{13}C_0)$ and the "background" $^{13}q_b = c_b\,(1 + \delta^{13}C_b)$ at the top boundary and in the inflow. In this work, $\delta^{13}C_0 = -0.014$ and $\delta^{13}C_b = -0.035$. The distribution of $^{13}q(x, z)$ with $^{13}\boldsymbol{k}$ in equation (A1) is then solved by conventional line iteration, and the distribution of methane $\delta^{13}C$ is subsequently calculated from $\delta^{13}C(x, z) = {}^{13}q(x, z)/q(x, z) - 1$.

## Acknowledgments

[54] The assistance of the officers and crews of R/Vs *M. S. Merian* and *L'Atalante* is greatly appreciated. We gratefully acknowledge the efforts of Peggy Wefers in carrying out the determination of methane carbon isotopes as well as her assistance on *L'Atalante*. We are also grateful for the many constructive comments of Jean-Luc Charlou and Marvin Lilley on the original manuscript. We thank David Hilton for editorial assistance. This work was supported by the Deutsche Forschungsgemeinschaft and is publication 35 of the priority program SPP 1144, "From Mantle to Ocean: Energy-, Material- and Life-cycles at Spreading Axes."

## References

Buller, S. (2008), Methane distributions at Logatchev hydrothermal field at 14°45′N on the Mid-Atlantic Ridge, M.S. thesis, 74 pp., Christian-Albrechts Uni., Kiel, Germany.

Charlou, J.-L., and J. P. Donval (1993), Hydrothermal methane venting between 12°N and 26°N along the Mid-Atlantic Ridge, *J. Geophys. Res.*, *98*, 9625–9642, doi:10.1029/92JB02047.

Charlou, J. L., Y. Fouquet, H. Bougault, J. P. Donval, J. Etoubleau, P. Jean-Baptiste, A. Dapoigny, P. Appriou, and P. A. Rona (1998), Intense $CH_4$ plumes generated by serpentinization of ultramafic rocks at the intersection of the 15°20′N fracture zone and the Mid-Atlantic Ridge, *Geochim. Cosmochim. Acta*, *62*, 2323–2333, doi:10.1016/S0016-7037(98)00138-0.

Charlou, J. L., J. P. Donval, Y. Fouquet, P. Jean-Baptiste, and N. Holm (2002), Geochemistry of high $H_2$ and $CH_4$ vent fluids issuing from ultramafic rocks at the Rainbow hydrothermal field (36°14′N, MAR), *Chem. Geol.*, *191*, 345–359, doi:10.1016/S0009-2541(02)00134-1.

Charlou, J. L., J. P. Donval, C. Konn, H. Ondreas, Y. Fouquet, P. Jean-Baptiste, and E. Fourré (2009), High production and fluxes of $H_2$ and $CH_4$ and evidence of abiotic hydrocarbon synthesis by serpentinization in ultramafic-hosted hydrothermal systems on the Mid-Atlantic Ridge, in *Diversity of Hydrothermal Systems on Slow-Spreading Ocean Ridges*, *Geophys. Monogr. Ser.*, edited by P. Rona et al., AGU, Washington, D. C., in press.

Cherkaschev, G. A., A. M. Ashadze, A. V. Gebruk, and E. M. Krylova (2000), New fields with manifestations of hydrothermal activity in the Logatchev area (14°N, Mid-Atlantic Ridge), *Interridge News*, *9*(2), 26–27.

Coleman, D. D., J. B. Risatti, and M. Schoell (1981), Fractionation of carbon and hydrogen isotopes by methane-oxidizing bacteria, *Geochim. Cosmochim. Acta*, *45*, 1033–1037, doi:10.1016/0016-7037(81)90129-0.

Cowen, J. P., X. Wen, and B. N. Popp (2002), Methane in aging hydrothermal plumes, *Geochim. Cosmochim. Acta*, *66*, 3563–3571, doi:10.1016/S0016-7037(02)00975-4.

de Angelis, M., M. D. Lilley, E. J. Olson, and J. A. Baross (1993), Methane oxidation in deep-sea hydrothermal plumes

of the Endeavour Segment of the Juan de Fuca Ridge, *Deep Sea Res., Part I*, *40*, 1169–1186, doi:10.1016/0967-0637(93)90132-M.

Douville, E., J. L. Charlou, E. H. Oelkers, P. Bienvenu, C. F. Jove Colon, J. P. Donval, Y. Fouquet, D. Prieour, and P. Appriou (2002), The Rainbow vent fluids (36°14′N, MAR): The influence of ultramafic rocks and phase separation on trace metal content in Mid-Atlantic Ridge hydrothermal fluids, *Chem. Geol.*, *184*, 37–48, doi:10.1016/S0009-2541(01)00351-5.

Farley, K. A., E. Maier-Reimer, P. Schlosser, and W. S. Broecker (1995), Constraints on mantle $^3$He fluxes and deep-sea circulation from an oceanic general circulation model, *J. Geophys. Res.*, *100*, 3829–3839, doi:10.1029/94JB02913.

Fouquet, Y., et al. (2008), Serpentine cruise–ultramafic hosted deposits on the Mid-Atlantic Ridge: First submersible studies on Aschadze 1 and 2, Logatchev 2 and Krasnov vent fields, *Interridge News*, *17*, suppl., 16–21.

Grant, N. J., and M. J. Whiticar (2002), Stable isotope evidence for methane oxidation in plumes above Hydrate Ridge, Cascadia Oregon Margin, *Global Biogeochem. Cycles*, *16*(4), 1124, doi:10.1029/2001GB001851.

Heeschen, K. U., R. S. Keir, G. Rehder, O. Klatt, and E. Suess (2004), Methane dynamics in the Weddell Sea determined via stable isotope ratios and CFC-11, *Global Biogeochem. Cycles*, *18*, GB2012, doi:10.1029/2003GB002151.

Holmes, M. E., F. J. Sansone, T. M. Rust, and B. N. Popp (2000), Methane production, consumption, and air-sea exchange in the open ocean: An evaluation based on carbon isotopic ratios, *Global Biogeochem. Cycles*, *14*, 1–10, doi:10.1029/1999GB001209.

Jean-Baptiste, P., E. Fourré, J.-L. Charlou, C. R. German, and J. Radford-Knoery (2004), Helium isotopes at the Rainbow hydrothermal site (Mid-Atlantic Ridge, 36°, 14′N), *Earth Planet. Sci. Lett.*, *221*, 325–335, doi:10.1016/S0012-821X(04)00094-9.

Jenkins, W. J., and W. B. Clarke (1976), The distribution of $^3$He in the western Atlantic Ocean, *Deep Sea Res.*, *23*, 481–494.

Joseph, J., and H. Sendner (1958), The horizontal diffusion in the ocean, *Ocean Dyn.*, *11*, 49–77, doi:10.1007/BF02020293.

Keir, R. S., J. Greinert, M. Rhein, G. Petrick, J. Sültenfuß, and K. Fürhaupter (2005), Methane and methane carbon isotope ratios in the northeast Atlantic including the Mid-Atlantic Ridge (50°N), *Deep Sea Res., Part I*, *52*, 1043–1070, doi:10.1016/j.dsr.2004.12.006.

Keir, R. S., O. Schmale, M. Walter, J. Sültenfuß, R. Seifert, and M. Rhein (2008), Flux and dispersion of gases from the "Drachenschlund" hydrothermal vent at 8° 18′ S, 13° 30′ W on the Mid-Atlantic Ridge, *Earth Planet. Sci. Lett.*, *270*, 338–348, doi:10.1016/j.epsl.2008.03.054.

Kinnaman, F. S., D. L. Valentine, and S. C. Tyler (2007), Carbon and hydrogen isotope fractionation associated with the aerobic microbial oxidation of methane, ethane, propane and butane, *Geochim. Cosmochim. Acta*, *71*, 271–283, doi:10.1016/j.gca.2006.09.007.

Lein, A. Y., D. V. Grichuk, E. G. Gurvich, and Y. A. Bogdanov (2000), A new type of hydrogen- and methane-rich hydrothermal solution in the rift zone of the Mid-Atlantic Ridge, *Dokl. Akad. Nauk*, *375*, 380–383. (English translation, *Dokl. Earth Sci.*, *375A*, 1391–1394, 2000.)

Lilley, M. D., D. A. Butterfield, E. J. Olson, J. E. Lupton, S. A. Macko, and R. E. McDuff (1993), Anomalous $CH_4$ and $NH_4^+$ concentrations at an unsedimented mid-ocean-ridge hydrothermal system, *Nature*, *364*, 45–47, doi:10.1038/364045a0.

Murton, B. J., L. J. Redbourn, C. R. German, and E. T. Baker (1999), Sources and fluxes of hydrothermal heat, chemicals and biology within a segment of the Mid-Atlantic Ridge, *Earth Planet. Sci. Lett.*, *171*, 301–317, doi:10.1016/S0012-821X(99)00157-0.

Nihous, G. C., and S. M. Masutani (2007), Notes on the modeling of methane in aging hydrothermal plumes, *J. Mar. Res.*, *65*, 789–812, doi:10.1357/002224007784219011.

Okubo, A. (1971), Oceanic diffusion diagrams, *Deep Sea Res.*, *18*, 789–802.

Polzin, K., J. Toole, J. Ledwell, and R. Schmitt (1997), Spatial variability of turbulent mixing in the abyssal ocean, *Science*, *276*, 93–96, doi:10.1126/science.276.5309.93.

Rehder, G., R. S. Keir, E. Suess, and M. Rhein (1999), Methane in the northern Atlantic controlled by microbial oxidation and atmospheric history, *Geophys. Res. Lett.*, *26*, 587–590, doi:10.1029/1999GL900049.

Rice, A. L., A. A. Gotoh, H. O. Ajie, and S. C. Tyler (2001), High-precision continuous-flow measurement of $\delta^{13}$C and $\delta$D of atmospheric $CH_4$, *Anal. Chem.*, *73*, 4104–4110, doi:10.1021/ac0155106.

Schmidt, K., A. Koschinsky, D. Garbe-Schönberg, L. M. de Carvalho, and R. Seifert (2007), Geochemistry of hydrothermal fluids from ultramafic-hosted Logatchev hydrothermal field, 15°N on the Mid-Atlantic Ridge: Temporal and spatial investigation, *Chem. Geol.*, *242*, 1–21, doi:10.1016/j.chemgeo.2007.01.023.

Scranton, M. I., and P. G. Brewer (1978), Consumption of dissolved methane in the deep ocean, *Limnol. Oceanogr.*, *23*, 1207–1213.

Sudarikov, S. M., and A. B. Roumiantsev (2000), Structure of hydrothermal plumes at the Logatchev vent field, 14°45′N, Mid-Atlantic Ridge: Evidence from geochemical and geophysical data, *J. Volcanol. Geotherm. Res.*, *101*, 245–252, doi:10.1016/S0377-0273(00)00174-8.

Sültenfuß, J., M. Rhein, and W. Roether (2009), The Bremen Mass Spectrometric Facility for the measurement of helium isotopes, neon, and tritium in water, *Isotopes Environ. Health Stud.*, *45*(2), 1–13.

Templeton, A. S., K.-H. Chu, L. Alvarez-Cohen, and M. E. Conrad (2006), Variable carbon isotope fractionation expressed by aerobic $CH_4$-oxidizing bacteria, *Geochim. Cosmochim. Acta*, *70*, 1739–1752, doi:10.1016/j.gca.2005.12.002.

Thurnherr, A. M. (2006), Diapycnal mixing associated with an overflow in a deep submarine canyon, *Deep Sea Res., Part II*, *53*, 194–216, doi:10.1016/j.dsr2.2005.10.020.

Thurnherr, A. M., K. J. Richards, C. R. German, G. F. Lane-Serff, and K. G. Speer (2002), Flow and mixing in the rift valley of the Mid-Atlantic Ridge, *J. Phys. Oceanogr.*, *32*, 1763–1778, doi:10.1175/1520-0485(2002)032<1763:FAMITR>2.0.CO;2.

Tsunogai, U., N. Yoshida, J. Ishibashi, and T. Gamo (2000), Carbon isotopic distribution of methane in deep-sea hydrothermal plume, Myojin Knoll Caldera, Izu-Bonin arc: Implications for microbial methane oxidation in the oceans and applications to heat flux estimation, *Geochim. Cosmochim. Acta*, *64*, 2439–2452, doi:10.1016/S0016-7037(00)00374-4.

Tsunogai, U., F. Nakagawa, T. Gamo, and J. Ishibashi (2005), Stable isotopic compositions of methane and carbon monoxide in the Suiyo hydrothermal plume, Izu-Bonin arc: Tracers for microbial consumption/production, *Earth Planet. Sci. Lett.*, *237*, 326–340, doi:10.1016/j.epsl.2005.05.042.

Valentine, D. L., D. C. Blanton, W. S. Reeburgh, and M. Kastner (2001), Water column methane oxidation adjacent to an area of active hydrate dissolution, Eel River Basin, *Geochim. Cosmochim. Acta*, *65*, 2633–2640, doi:10.1016/S0016-7037(01)00625-1.

Walker, S. L., E. T. Baker, G. J. Massoth, and R. N. Hey (2004), Short-term variations in the distribution of hydrothermal plumes along a superfast spreading center, East Pacific Rise, 27°30′–32°20′S, *Geochem. Geophys. Geosyst.*, *5*, Q12005, doi:10.1029/2004GC000789.

Welhan, J. A. (1988), Origins of methane in hydrothermal systems*Chem. Geol.*, *71*, 183–198, doi:10.1016/0009-2541(88)90114-3.

Young, D. M., and R. T. Gregory (1973), *A Survey of Numerical Mathematics*, vol. II, 1099 pp., Addison-Wesley, Reading, Mass.

Zhou, H. Y., Z. J. Wu, X. T. Peng, L. Jang, and S. Tang (2007), Detection of methane plumes in the water column of Logatchev hydrothermal vent field, Mid-Atlantic Ridge, *Chin. Sci. Bull.*, *52*, 2140–2146, doi:10.1007/s11434-007-0285-y.